J|A|C|S ARTICLES

Published on Web 08/26/2009

Crystal Structure of Ammonia Monohydrate Phase II

A. Dominic Fortes,*,†,‡ Emmanuelle Suard,§ Marie-Hélène Lemée-Cailleau,§ Christopher J. Pickard,|| and Richard J. Needs⊥

Centre for Planetary Sciences at UCL/Birkbeck, Gower Street, London, WC1E 6BT, United Kingdom, Department of Earth Sciences, University College London, Gower Street, London, WC1E 6BT, United Kingdom, Institut Laue-Langevin, BP156, 38042 Grenoble cedex 9, France, Department of Physics and Astronomy, University College London, Gower Street, London, WC1E 6BT, United Kingdom, and Theory of Condensed Matter Group, Cavendish Laboratory, Department of Physics, University of Cambridge, Cambridge CB3 0HE, United Kingdom

Received June 26, 2009; E-mail: andrew.fortes@ucl.ac.uk

Abstract: We have determined the crystal structure of ammonia monohydrate phase II (AMH II) employing a combination of *ab initio* computational structure prediction and structure solution from neutron powder diffraction data using direct space methods. Neutron powder diffraction data were collected from perdeuterated AMH II using the D2B high-resolution diffractometer at the Institut Laue-Langevin. AMH II crystallizes in space-group P*bca* with 16 formula units in a unit-cell of dimensions $a = 18.8285(4)$ Å, $b = 6.9415(2)$ Å, $c = 6.8449(2)$ Å, and $V = 894.61(3)$ Å^3 [$\rho_{calc}^{deuterated} = 1187.56(4)$ kg m^{-3}] at 502 MPa, 180 K. The structure is characterized by sheets of tessellated pentagons formed by orientationally ordered O−D···O, O−D···N, and N−D···O hydrogen-bonds; these sheets are stacked along the *a*-axis and connected by N−D···O hydrogen bonds alone. With the exception of the simple body-centered-cubic high-pressure phases of ammonia monohydrate and ammonia dihydrate, this is the first complex molecular structure of any of the high-pressure stoichiometric ammonia hydrates to be determined. The powder structure solution is complemented by an *ab initio* structure prediction using density functional theory which gives an almost identical hydrogen bonding network.

1. Introduction

The water−ammonia system is of interest to physical chemists since it represents a natural laboratory in which to observe the behavior of materials that contain a mixture of homonuclear and heteronuclear hydrogen bonds. The end-member phases (water ice and solid ammonia), and the stoichiometric hydrates, ammonia dihydrate ($NH_3 \cdot 2H_2O$, ADH), ammonia monohydrate ($NH_3 \cdot H_2O$, AMH), and ammonia hemihydrate ($NH_3 \cdot {}^1/_2H_2O$, AHH) are therefore model systems for understanding far more complex hydrogen-bonded molecules. The water−ammonia system is also of considerable interest to planetary scientists, since astronomical observations and cosmochemical models indicate that ammonia may be a significant component of the outer solar system volatile inventory.[1,2] Although there is some difference of opinion regarding the ammonia yield from various condensation models,[3] and indeed the fate of that ammonia once accreted into large bodies such as Titan,[4] it remains among the most plausible planetary "antifreeze" agents, and its physical properties under the appropriate conditions (roughly 0−5 GPa, 100−300 K) must be known for it to be accommodated in planetary models. The pressure melting curve and the polymorphism of the stoichiometric ammonia hydrates have implications for the internal structure of large icy satellites like Titan, leading to phase layering and the possible persistence of deep subsurface oceans,[5−9] the latter being sites of high astrobiological potential.[10,11] Aqueous ammonia is also a candidate substance involved in cryomagmatism on Titan;[12,13] the melting behavior, and densities of liquids and solids, in the ammonia−water system must be known to properly model the partial melting and vertical propagation of such a cryomagma through a planetary crust. Although cosmochemical models indicate that ADH is the most likely solid phase to be found in the outer solar system, it has been shown[14,15] that ADH becomes unstable with respect to a mixture of AMH + ice under pressures of just a few hundred MPa, equivalent to depths of a few hundred kilometers in a Titan-sized body. Upon warming at 550 MPa, the high-pressure phase ADH II breaks down to the high-

† Centre for Planetary Sciences at UCL/Birkbeck.
‡ Department of Earth Sciences, University College London.
§ Institut Laue-Langevin.
|| Department of Physics and Astronomy, University College London.
⊥ Cavendish Laboratory, Department of Physics, University of Cambridge.

(1) Lewis, J. S.; Prinn, R. G. *Astrophys. J.* **1980**, *238*, 357–364.
(2) Prinn, R. G.; Fegley, Jr, B. *Astrophys. J.* **1981**, *249*, 308–317.
(3) Mousis, O.; Gautier, D.; Bocklée-Morvan, D. *Icarus* **2002**, *156* (1), 162–175.
(4) Fortes, A. D.; Grindrod, P. M.; Trickett, S. K.; Vočadlo, L. *Icarus* **2007**, *188* (1), 139–153.
(5) Grasset, O.; Sotin, C. *Icarus* **1996**, *123* (1), 101–112.
(6) Grasset, O.; Sotin, C.; Dechamps, F. *Planet. Space Sci* **2000**, *48* (7−8), 617–636.
(7) Grasset, O.; Pargamin, *Planet. Space Sci.* **2005**, *53* (4), 371–384.
(8) Sohl, F.; Hussmann, H.; Schwentker, B.; Spohn, T.; Lorenz, R. D. *J. Geophys. Res. Planets* **2003**, *108* (E12), article 5130.
(9) Lorenz, R. D.; Stiles, B. W.; Kirk, R. L.; Allison, M. D.; Del Marmo, P. P.; Iess, L.; Lunine, J. I.; Ostro, S. J.; Hensley, S. *Science* **2008**, *319*, 1649–1651.
(10) Fortes, A. D. *Icarus* **2000**, *146* (2), 444–452.
(11) Raulin, F. *Space Sci. Rev.* **2008**, *135* (1−4), 37–48.
(12) Kargel, J. S. *Icarus* **1992**, *100* (2), 556–574.
(13) Lopes, R. M. C.; et al. *Icarus* **2007**, *186* (2), 395–412.

 10.1021/ja9052569 CCC: $40.75 © 2009 American Chemical Society

pressure phase II of AMH which is the subject of this paper; AMH II has also been observed to coexist with ADH II after melting of ADH I at 450 MPa, 179 K, and subsequent refreezing. Another high-pressure phase, ADH IV also breaks down to AMH when warmed at pressures of 3−6 GPa. Hence, the monohydrate may be of direct relevance to the internal dynamics of icy satellites, in our own solar system, and in exoplanetary systems.

At atmospheric pressure ammonia monohydrate crystallizes in an orthorhombic phase below the congruent melting point at 194.15 K.[16] The structure of this low-pressure phase, AMH I, was solved in space-group $P2_12_12_1$ ($Z = 4$) using single-crystal X-ray diffraction data at 113 K,[17] and subsequently refined from neutron powder diffraction measurements of the deuterated isotopologue at 110 K.[18]

The first visual and Raman scattering observations made using diamond anvil cells indicated that AMH possessed no high-pressure polymorphs;[19] however, dilatometric studies established the existence of a high-pressure phase, AMH II, stable above 340 MPa at 195 K.[20−22] Shortly afterward, a neutron powder diffraction pattern of this phase, collected at 508.9 MPa, was reported from studies using a gas pressure cell on the POLARIS diffractometer at ISIS.[23] Their experimental report states that the diffraction pattern was indexed with an orthorhombic ($Z = 16$) unit cell with a volume of 750 Å^3 (the proposed unit-cell is not cited). This would require the volume change, $\Delta V/V$, at the AMH I → II transition to be −20%, which is exceptionally large, although not implausible; the ice Ih → II and Ih → III transitions have $\Delta V/V \approx -20\%$. However, this AMH II indexing has since been shown by Fortes et al.[15] to be incorrect. High resolution neutron powder patterns of deuterated AMH II mixed with ammonia dihydrate II (ADH II) and/or ice II have been collected by one of us (ADF) using the HRPD, OSIRIS, and PEARL/HiPr diffractometers at ISIS; these mixtures were typically formed either by the melting of ammonia dihydrate phase I at 450 MPa (179 K) and subsequent refreezing of the aqueous solution or by the decomposition of ammonia dihydrate phase II at 550 MPa. The diffraction patterns of high-pressure ammonia monohydrate were indexed with an orthorhombic unit cell: the unit-cell dimensions determined by LeBail structure-less profile refinement are, $a = 18.8680(2)$ Å, $b = 6.9477(1)$ Å, and $c = 6.8589(1)$ Å at 443 MPa, 174 K. Comparison with the AMH I compression data of Loveday and Nelmes[24] showed that this powder indexing could *only* be consistent with 16 formula units per unit-cell, and a volume change at the AMH I → II transition of approximately −6%. The systematic absences pointed unambiguously to a primitive unit-cell with an *a*-glide parallel to (001), and a *c*-glide parallel to (010), but it was not possible to determine the symmetry element parallel to (100). The possible space-groups for this phase were, therefore, P*cca*, P*nca* and P*bca*, the latter being the most frequently occurring of the three among inorganic crystals.

Attempts using the FOX code[25,26] to solve the structure of AMH II using the available mixed-phase time-of-flight neutron powder data failed to produce any sensible results. However, Pickard and Needs[27] have reported a structure prediction technique which requires no more information than the number and identities of the atoms in the unit-cell and, in addition, allows the application of constraints which may be determined from experimental data or other considerations; we describe an application of this method to the AMH II structure solution. The neutron powder diffraction data for AMH II presented here were collected with, the objective of verifying the structure prediction algorithm using the best possible single-phase measurements.

2. Methods

2.1. Experimental Method: Neutron Powder Diffraction. The experiment was carried out on a sample of nominal composition $ND_3 \cdot D_2O$ (AMH) prepared by condensing ND_3 gas (Aldrich Chemicals Co., 99 atom % D) into an evacuated glass bulb which was cooled to 215 K in a bath of acetone cooled by dry ice.[28] The bulb was then weighed and the contents diluted to the appropriate stoichiometry with D_2O (Aldrich Chemicals Co., 99 atom % D). Gravimetric analysis indicated that the composition of the solution was 49.96 wt. % ND_3; the ideal AMH stoichiometry is 50.03 wt. % ND_3. So as to minimize the loss of volatile ND_3, the solution was stored in a cabinet-freezer for ∼60 h and then transported from London to Grenoble in a dewar containing water-ice deeply cooled by liquid nitrogen. The specimen remained in this dewar for ∼24 h prior to the loading of the pressure vessel.

Neutron powder diffraction data were collected using the D2B high-resolution diffractometer[29] at the Institut Laue-Langevin, Grenoble, France. High pressures were achieved using a $Ti_{66}Zr_{34}$ null-scattering-alloy gas cell (ILL code 03PG50TZ7: sample Ø7 mm by 30 mm high), connected to a helium gas intensifier. Temperature control was achieved using a standard ILL 50 mm aluminum-tailed "Orange" cryostat mounted on the D2B sample platform. The empty pressure vessel was suspended in a bath of liquid nitrogen and small tufts of silica wool (total mass of order 0.1 g) were dropped into the sample space; the purpose of this wool was to promote the formation of a more randomly oriented polycrystalline mass from the liquid specimen, rather than a few large single crystals. The specimen was introduced into the pressure cell using a cooled glass pipette, where it froze immediately: the cell was then quickly screwed onto the cryostat center stick, pressurized to 100 bar (10 MPa) and mounted in the cryostat.

AMH I was crystallized in the pressure vessel and subsequently compressed in 25 MPa increments along the 180 K isotherm up to

(14) Fortes, A. D.; Wood, I. G.; Alfredsson, M.; Vočadlo, L.; Knight, S.; Marshall, W. G.; Tucker, M. G.; Fernandez-Alonso, F. *High Press. Res.* **2007**, *27* (2), 201–212.
(15) Fortes, A. D.; Wood, I. G.; Vočadlo, L.; Knight, K. S.; Marshall, W. G.; Tucker, M. G.; Fernandez-Alonso, F. *J. Appl. Cryst.* **2009**, *42* (5), published online, DOI: 10.1107/S0021889809027897.
(16) Hildenbrand, D. L.; Giauque, W. F. *J. Am. Chem. Soc.* **1953**, *75* (12), 2811–2818.
(17) Olovsson, I.; Templeton, D. H. *Acta Crystallogr.* **1959**, *12*, 827–832.
(18) Loveday, J. S.; Nelmes, R. J. Structural studies of ammonia hydrates. In *Science and Technology of High Pressure: Proceedings of AIRAPT-17*; Manghnani, M. H., Nellis, W. J., Nicol, M. T., Eds.; Universities Press: Hyderabad, India, 2000; pp 133−136.
(19) Koumvakalis, A. *High pressure study of ammonia monohydrate.* PhD Thesis, University of California, Los Angeles, 1988.
(20) Kargel, J. S.; Hogenboom, D. L. *Proc. Lunar Planet. Sci.* **1995**, *26*, 725–726.
(21) Hogenboom, D. L.; Kargel, J. S.; Holden, T. C.; Buyyounouski, M. *Proc. Lunar Planet. Sci.* **1995**, *26*, 613–614.
(22) Hogenboom, D. L.; Kargel, J. S.; Consolmagno, G. J.; Holden, T. C.; Lee, L.; Buyyounouski, M. *Icarus* **1997**, *128* (1), 171–180.
(23) Nelmes, R. J.; Loveday, J. S. *ISIS Experimental Report RB9859. CCLRC Rutherford Appleton Laboratory*, 1998 (www.isis.rl.ac.uk/ISIS98/reports/9859.pdf).
(24) Loveday, J. S.; Nelmes, R. S. *High Press. Res.* **2004**, *24* (1), 45–55.
(25) Favre-Nicolin, V.; Černý, R. *J. Appl. Crystallogr.* **2002**, *35*, 734–743.
(26) Favre-Nicolin, V.; Černý, R. *Z. Kristallogr.* **2004**, *219*, 847–856.
(27) Pickard, C. J.; Needs, R. J. *Phys. Rev. Lett.* **2006**, *97*, article 045504.
(28) This work was done at, and using equipment supplied by, the STFC ISIS Facility, Harwell Science and Innovation Campus, Chilton, United Kingdom.
(29) Suard, E.; Hewat, A. *Neutron News* **2001**, *12* (4), 30–33.

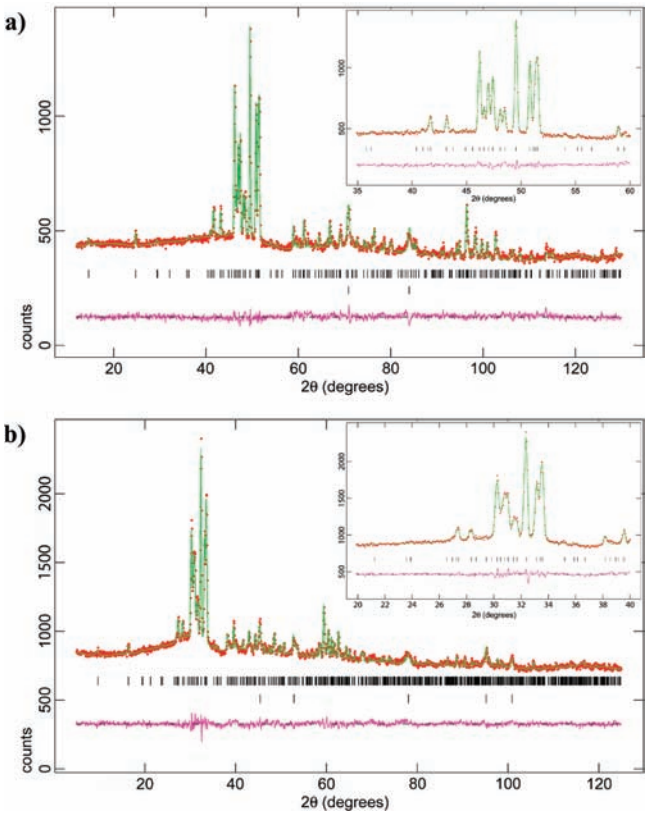

Figure 1. Diffraction data acquired at 502 MPa, 180 K at (a) $\lambda = 2.39845$ Å, and (b) $\lambda = 1.59432$ Å. In both panels, the red points are the measured neutron counts, the green line represents the Rietveld structural refinement (see section 3.3), and the pink line beneath the diffraction pattern is the difference curve. The expected positions of Bragg reflections are shown by vertical black tick marks; the upper set are for AMH II, and the lower set are for copper, the latter being a component in the Bridgman seal of the pressure vessel. In both panels, the insets show an expanded portion of the data to illustrate the improved *d*-spacing resolution in the vicinity of the strongest reflections afforded by the longer neutron wavelength.

the maximum rated pressure of the gas vessel, 500 MPa. The transformation of AMH I to AMH II occurred over an interval of approximately 90 min at 350 MPa: measurements made below, during, and above the phase transition are reported elsewhere.[30]

At 502 MPa, two long integrations were made in order to provide data suitable for testing structural models of AMH II. The first 7 h integration was made using the "high-resolution" mode of D2B (Ge [335] monochromated radiation, $\lambda = 1.59432$ Å, horizontal slits reduced to 100 mm, average resolution $\Delta d/d < 5 \times 10^{-4}$). The second 5 h integration was made using one of the longer wavelength options (Ge [331] monochromated radiation, graphite filtered, $\lambda = 2.39845$ Å, 200 mm horizontal slits), the purpose of which was to disperse the Bragg reflections observed at lower angles over a broader 2θ range so as to improve the resolution of several closely spaced peaks in the data (compare the insets to Figure 1a and b). At the end of the experiment the cell was depressurized and evacuated, and a 90 min integration was made with the empty TiZr cell to characterize the very strong background contribution made by the cell body and weak Bragg reflections from the extruded copper Bridgman seal.

The raw data files were exported as GSAS format DAT files and analyzed using the Rietveld method[31] implemented in the GSAS/EXPGUI software package (Larsen and Von Dreele, 2000: Toby, 2001).[32,33] For both data sets we used only those counts from one-third of the 300 mm-high detectors centered on their equatorial plane; this provides us with data from the most sharply focused portions of the Debye−Scherrer rings on the detectors and thus the highest angular resolution.

2.2. Computational Method: AMH II *ab initio* Structure Prediction. Pickard and Needs[27] have developed a method for determining crystal structures based on *ab initio* density functional theory calculations. This method has been applied to a number of materials, including compressed ices of water[34] and ammonia.[35] In the absence of pre-existing crystallographic information the method proceeds by generating random unit-cell vectors and normalizing the unit-cell volume to a reasonable value for the system under consideration; the required atoms are then inserted at random positions within the unit-cell, and the atomic positions and unit-cell size and shape are relaxed until a minimum in the energy (or, at finite pressures, the enthalpy) is reached. This process is repeated with new random starting structures until a satisfactory low-energy crystal structure is obtained. A rule of thumb for deciding when to terminate the search is that the lowest-energy structure should be obtained more than once and that any known structures of the system should be obtained. In practice, it is often necessary to perform searches with different numbers of atoms in the unit-cell. In the case of the work described here, the initial step of random unit-cell generation was obviated by the use of experimentally determined unit-cell parameters.

The *ab initio* calculations were performed using the CASTEP plane wave code[36] with the Perdew−Burke−Ernzerhof (PBE) generalized gradient approximation (GGA) exchange-correlation functional[37] and ultrasoft pseudopotentials.[38] We used a plane-wave basis set cutoff energy of 340 eV. Only a sparse sampling of the Brillouin zone is required to obtain accurate results because the unit-cell is large and the material is an insulator; we used a single $\vec{k}$-point corresponding to ($^1/_4$,$^1/_4$,$^1/_4$) of the reciprocal lattice vectors of the unit-cell.

The *ab initio* search calculations were performed after the experimental work on mixtures of deuterated AMH II, ADH II, and ice II,[15] but prior to the experiment on nominally phase-pure AMH. The unit-cell parameters and the likely space groups (P*cca*, P*nca* and P*bca)* were available[15] and it was assumed that the crystal retains the molecular character of the low-pressure phase; that is, it consists of weakly hydrogen-bonded NH_3 and H_2O molecules. We used this information to simplify the search problem. The unit-cell parameters were fixed at the experimentally derived values $a = 18.8680$ Å, $b = 6.9477$ Å, and $c = 6.8589$ Å obtained at 443 MPa, 174 K[15] and $H_2NH\cdots OH_2$ units were inserted at random, rejecting initial configurations in which the molecules overlapped strongly. We performed searches within each of the three candidate space groups, using between one and two hundred configurations for each space-group. Each of the space-groups contains eight symmetry operations, such that the asymmetric unit contains two formula units. Using the experimentally derived information greatly reduces the size of the parameter space that must be searched. The search within space-group P*bca* gave the lowest enthalpy structures, twice yielding the most stable structure found overall; the atomic coordinates and interatomic distances and angles are given in the Supporting Information.

(30) Fortes, A. D.; Suard, E.; Lemée-Cailleau, M.-H.; Pickard, C. J.; Needs, R. J. *J. Chem. Phys.* 2009. submitted.
(31) Rietveld, H. M. *J. Appl. Crystallogr.* **1969**, *2* (2), 65–71.
(32) Larsen, A. C.; Von Dreele, R. B. *General Structure Analysis System (GSAS). Los Alamos National Laboratory Report LAUR 86−748*; Los Alamos, NM, 2000 (http://www.ncnr.nist.gov/xtal/software/gsas.html).
(33) Toby, B. H. *J. Appl. Crystallogr.* **2001**, *34*, 210–213.
(34) Pickard, C. J.; Needs, R. J. *J. Chem. Phys.* **2007**, *127*, article 245503.
(35) Pickard, C. J.; Needs, R. J. *Nat. Mater.* **2008**, *7*, 775–779.
(36) Clark, S. J.; Segall, M. D.; Pickard, C. J.; Hasnip, P. J.; Probert, M. I. J.; Refson, K.; Payne, M. C. *Z. Kristallogr.* **2005**, *220*, 567–570.
(37) Perdew, J. P.; Burke, K.; Ernzerhof, M. *Phys. Rev. Lett.* **1996**, *77*, 3865–3868.
(38) Vanderbilt, D. *Phys. Rev. Lett.* **1990**, *41*, 7892–7895.

3. Results

3.1. Solution and Refinement of the AMH II Crystal Structure. An initial survey of the newly acquired AMH II neutron powder data, the useful parts of which extend to $2\theta = 10.05°$ ($d = 13.669$ Å) at $\lambda = 2.39845$ Å, and $2\theta = 4.05°$ ($d = 22.739$ Å) at $\lambda = 1.59432$ Å, revealed no evidence of the 010 reflection, expected at $2\theta = 19.884°$ (with $\lambda = 2.39$ Å), or the 011 reflection, expected at $2\theta = 28.478°$ (with $\lambda = 2.39$ Å). Although these reflections may be below the noise level, their apparent absence supports the assignment of P*bca* as the correct space-group over P*nca* and P*cca*, in agreement with the lowest-energy candidate structure that emerged from the *ab initio* structure prediction process.

Attempts to solve the atomic structure of AMH II were made in space-groups P*bca*, P*nca*, and P*cca* from the data set acquired at 502 MPa, 180 K, using the parallel tempering algorithm implemented in FOX, version 1.6.99.[25,26] Inputs for the solution process were the background-subtracted diffraction data collected at $\lambda = 2.39845$ Å, along with profile coefficients determined by LeBail fitting[39,40] to the data with GSAS/Expgui, and definitions of the molecular fragments (D_2O and ND_3) in the asymmetric unit in the form of Z-matrices, which FOX was instructed to treat as rigid bodies. Initial runs of 3 million trials for each space-group were done, in which the crystal structure was optimized against the measured diffraction pattern; these revealed that the cost functions of the solutions in space-groups P*nca* and P*cca* were, respectively, 1.9 and 2.6 times larger than those of solutions obtained in space-group P*bca*. A further five runs of 3 million trials were then run solely in space-group P*bca*; this yielded three solutions which were structurally indistinguishable and another two which were similar. The structure with the lowest overall cost function was exported as a CIF file to form the basis for Rietveld refinement with GSAS.

Inspection of this empirically derived structure revealed that it was almost identical to the lowest energy computationally derived candidate; each represents one of two possible end-members derived by ordering the orientation of water molecules along the O−D···O chains (see section 3.2). to determine whether the structure of AMH II adopts one of these two possible orientationally ordered variants, or is a combination of the two variants (i.e., it is disordered), we have carried out a Rietveld refinement of the various structural models to the newly acquired powder data.

In all three models, the structural refinement was done using the same rather stiff bond-length and bond-angle restraints (the weighting factor of the restraint was set to FACTR = 200 in GSAS): the O−D bonds and D-D distances in the water molecules were fixed at 0.990(5) Å, and 1.570(5) Å, respectively, the latter forcing ∠D−O−D to be 104.9(9)°; the N-D bonds and D-D distances in the ammonia molecules were fixed at 1.000(5) Å, and 1.625(5) Å, respectively, the latter forcing ∠D−N−D to be 108.7(9)°. Using both the 2.39845 Å and the 1.59432 Å data sets combined, the background in each histogram was fixed using a 36-term Chebyschev polynomial to model the complex incoherent contribution from the TiZr body of the pressure vessel, while the scale factors, the phase fractions (AMH II and copper), and peak profile coefficients (Gaussian and Lorentzian terms, plus asymmetry for AMH II, only the Lorentzian terms and asymmetry for the copper) were refined. Hard constraints were used to force like atoms (O, N, water deuterons and ammonia deuterons) to experience equal shifts in their isotropic displacement parameters, U_{iso}.

Structural refinement of the three models yielded a clear distinction in the goodness-of-fit criteria (Rietveld powder statistics, Rp and χ^2), with the ordered model obtained from the *ab initio* prediction algorithm fitting least well, the ordered model obtained from the powder structure solution fitting best, and the model with half-occupied deuteron sites along the O−O vectors falling between the two. To provide a bench-mark by which to judge the quality of the fit, a structure-less LeBail profile refinement was carried out, varying only the unit-cells of AMH II and copper, and their peak profile coefficients. Despite being a rigidly constrained model without anisotropic displacement factors, the empirically derived structure provides a remarkably good fit to the data; indeed some of the largest excursions in the difference curves (Figure 1a and b) are due to Cu and not AMH II.

Since it was clear that the AMH II structure adopted one particular ordered structure, this was selected for further refinement using GSAS. The soft bond-length and bond-angle restraints were switched off first, followed sequentially by the hard constraints on U_{iso} shifts, and then by refinement of spherical harmonic texture coefficients. The texture coefficients, refined to sixth order yielded a small improvement in the goodness-of-fit criteria (Rp dropped from 1.31 to 1.26%; χ^2 dropped from 2.271 to 2.122), and a quite small texture index, 1.10(1), indicative of a relatively weakly oriented powder. However, there was a significant improvement in the O−D and N−D bond lengths, some of which were anomalously short in the absence of the texture correction. Given that the specimen was grown from an amorphous solid inside the pressure vessel, it is not surprising that a small amount of preferred orientation is present (certainly much less than we have seen in some other similar experiments). The last refinement cycles proceeded smoothly and converged quickly to a stable solution, which is the subject of the next section. The Rietveld powder statistics of the unrestrained fit are reported in the electronic Supporting Information.

3.2. Description of the AMH II Crystal Structure. As shown in Figure 2, the structure of AMH II contains water molecules that are hydrogen bonded to form a square crankshaft chain extending infinitely along the *c*-axis. Each D_2O corner of the crankshaft donates a hydrogen bond to an ammonia molecule, alternately above and below the plane of the chain. Every other ammonia (denoted N2) donates one hydrogen bond back to the opposing corner of the same water−water chain, thereby forming a pentagonal ribbon, which possesses a boat conformation when viewed along the *c*-axis (see Figure 3b). Figure 2 also reveals that there are two possible ways of ordering the hydrogen bonds in the water−water chain: the first (Figure 2a and b) has the hydrogen bonding across the ammonia at the apex of the pentagon "flowing" in the *same* direction (i.e., all "flowing" right to left) as the hydrogen bonding in the water−water chain; the second (Figure 2c and d) has the hydrogen bonding across the ammonia at the apex of the pentagon "flowing" in the *opposite* direction (right to left) from the bonding in the water−water chain (left to right).

Clearly, it is also possible to have a completely disordered model, which may be seen as a superposition of the two ordered states, having half-occupied hydrogen sites between adjacent water molecules. Equally, a spectrum of partially ordered models are also possible without the need to change the unit-cell

(39) LeBail, A.; Duroy, H.; Fourquet, J. L. *Mater. Res. Bull.* **1988**, *23*, 447–452.
(40) LeBail, A. *Powder Diff.* **2005**, *20* (4), 316–326.

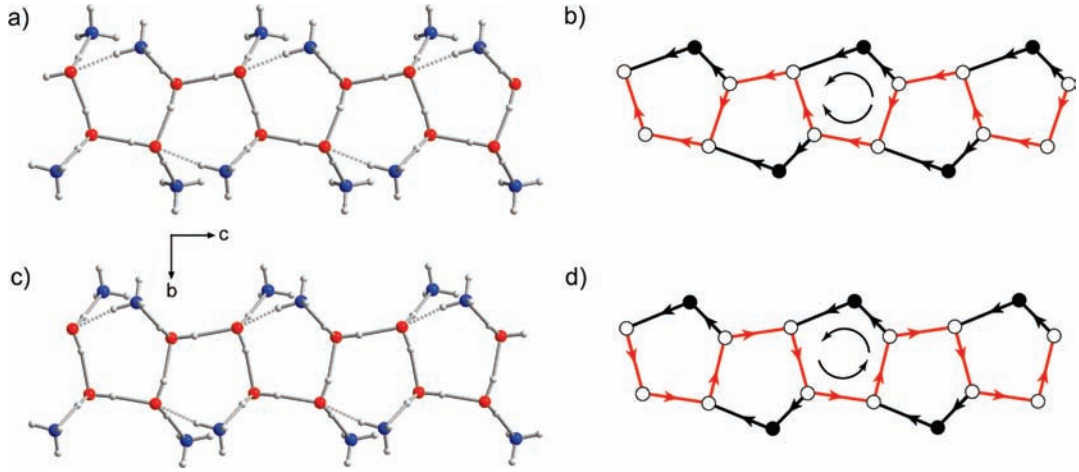

Figure 2. Hydrogen bond ordering scheme in the computationally derived model of the AMH II structure, depicted as a ball-and-stick model in (a) and schematically in (b): the hydrogen bond ordering scheme in the empirically derived model is shown in (c) and (d). Red arrows in (b) and (d) show the direction of hydrogen-bond donation in the water−water chain, and the black arrows show the direction of H-bond donation to and from the N2 atom at the apex of the pentagon.

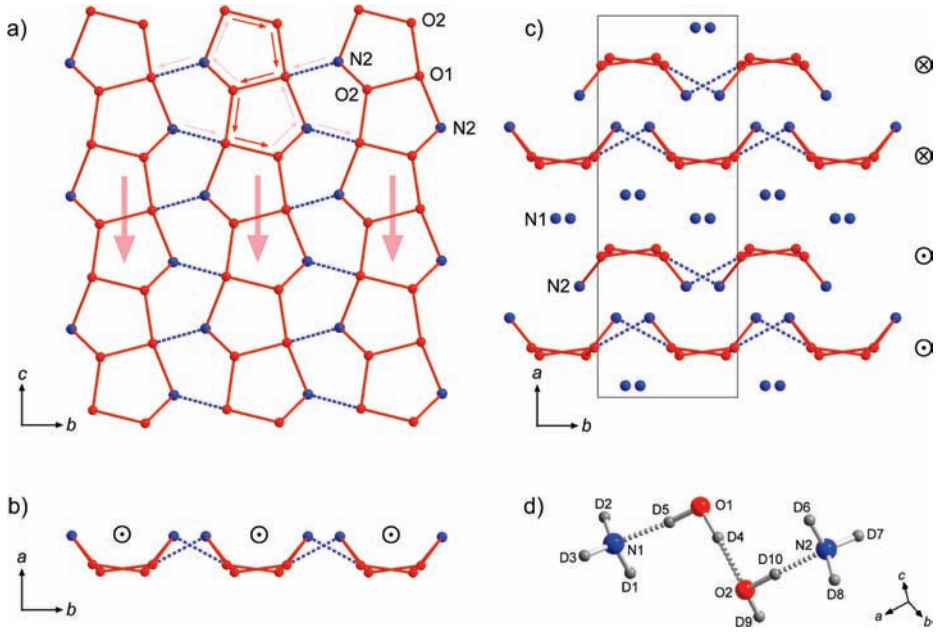

Figure 3. Molecular connectivity and packing in the AMH II structure. Oxygen atoms are shown in red, nitrogen in blue, and deuterium in gray; see text for further discussion of notation.

symmetry. The ordering scheme with same-sense bonding across the pentagon (Figure 2a and b) was obtained by *ab initio* structure prediction, and the scheme with opposite-sense bonding across the pentagon (Figure 2c and d) was obtained by powder structure solution. As described in the previous section, Rietveld refinement shows that the latter *fully proton ordered* model gives the best fit to the data. The refined atomic coordinates of this structure, and of the computationally derived model, along with selected interatomic distances and angles, are provided in the electronic supplementary tables, and the accompanying CIF file.

Figure 3a shows a view of the pentagonal ribbons down the *a*-axis (with the *c*-axis vertical). The direction of the O−D···O H-bonds is shown by the red arrows (the return bonding across the pentagonal apex is indicted by small pink arrows), resulting in a net-directionality indicated by the large pink arrows. Adjacent ribbons lying in the same plane bond to one another roughly along the *b*-axis (dashed blue bonds) to form a pentagonally tessellated sheet. A view of this sheet along the *c*-axis (with the *a*-axis vertical) is shown in Figure 3b; note the boat conformation of individual pentagonal ribbons, and note the symbol (⊙) indicating that the direction of hydrogen bonds in the crankshafts is coming out of the plane of the illustration.

The packing of these sheets is depicted in Figure 3c, also viewed along the *c*-axis, with the *a*-axis vertical and the *b*-axis horizontal. The glide planes generate adjacent offset sheets, with the hydrogen bonding along the crankshafts coming out of the plane of the illustration (⊙), related by the center of symmetry to sheets with the hydrogen bonding along the crankshafts going into the plane of the illustration (⊗).

This structure bears a number of intriguing similarities to the tetragonal argon clathrate (TAC) structure described by Manakov et al.,[41] which appears only to be stable above ∼900 MPa.

(41) Manakov, A.Yv.; Voronin, V. I.; Kurnosov, A. V.; Teplykh, A. E.; Komarov, V. Yu.; Dyadin, Yu. A. *J. Incl. Phenom. Macrocycl. Chem.* **2004**, *48*, 11–18.

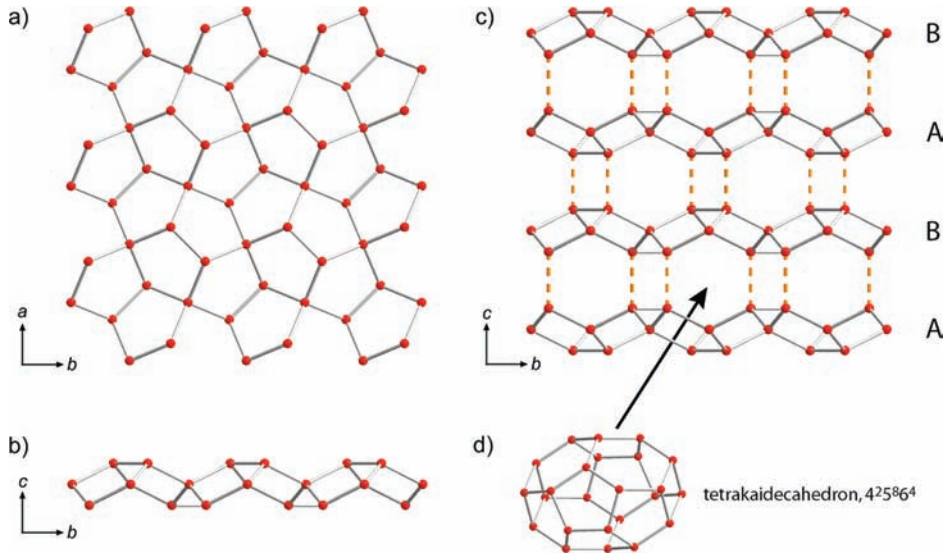

Figure 4. Molecular connectivity and packing in the tetragonal argon clathrate structure described by Manakov et al.[41] and represented in the same manner as AMH II in Figure 3.

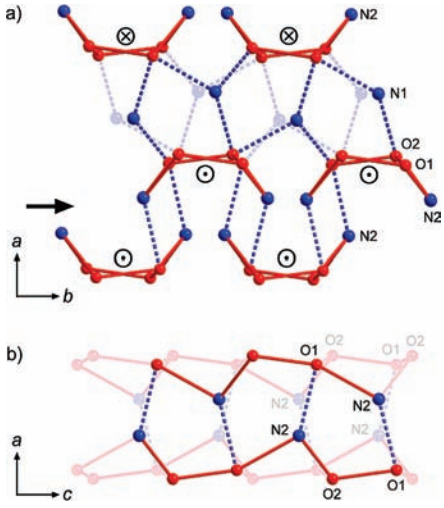

Figure 5. Hydrogen bonding between neighboring pentagonally tessellated sheets, viewed along the *c*-axis in (a), showing the difference in connectivity, through N1, between sheets with the opposite sense of hydrogen bond directionality (⊗ adjacent to ⊙), and between sheets with the same sense of hydrogen bond directionality (⊙ adjacent to ⊙), via N2. In part (b) is shown the view along the *b*-axis (shown in (a) with the bold arrow), illustrating the repeated pentagonal motif.

This clathrate consists of pentagonally tessellated sheets of water molecules (Figure 4a), virtually identical in terms of connectivity to the sheets in AMH II; the hydrogen bonds in the tetragonal clathrate, however, are fully disordered. The principal difference with AMH II is that the sheets in TAC have identical upper and lower surfaces (Figure 4b); in AMH II the sheets have a distinct "top" and "bottom". The sheets in TAC stack along the *c*-axis (Figure 4c), related by mirror planes rather than glides, and thereby form large 14-sided polyhedral cavities (Figure 4d) each of which may be occupied by up to three argon atoms.

The pentagonal ring motif is prevalent not only within the sheet structure of AMH II (Figure 3a) but between the sheets (Figure 5). There is an extensive literature describing the role of pentagonal clusters—and clathrate-like structures—in liquid water,[42,43] both from a computational[44] and an experimental perspective;[45] most recently, stable pentagonal rings of water were formed on a copper substrate.[46]

The structure is characterized by strong (i.e., short) hydrogen bonds donated by water molecules to both O and N, of length ~ 1.8 Å, and weaker (i.e., longer) hydrogen bonds donated by ammonia molecules to both O and N, of length 2.1−2.3 Å. The H-bonds donated by D_2O are generally less strained (i.e., they are more linear), with O−D···X angles between 169−177° (average = 173.25°). In common with solid ammonia,[47] the H-bonds donated by ND_3 are all considerably less linear, with N−D···X angles between 152−168° (average = 161.8°). These bond lengths and angles are very similar to those found in AMH I at atmospheric pressure.[18] The logical consequence of reducing the volume while maintaining the length of the bonded nearest-neighbor contacts is that the nonbonded nearest neighbor shells must shrink. In water ice, where the volume change from ice Ih to ice II or ice III is ~20%, the nearest nonbonded O−O contacts shrink from ~4.5 Å to as little as 3.2 Å. In AMH II the volume change at the transition is a more modest 4.6%[30] so we should not expect such a dramatic collapse of the nonbonded shells. Figure 6 illustrates the chain structures in AMH I and AMH II along with the radial O−O distances. Clearly, the bonded O−O contacts at ~2.8 Å do not change, but the first shell of nonbonded O−O contacts at ~4.5 Å moves in as close as 4.09 Å; this is due to the change in geometry of the O−O chains from a zigzag arrangement to a crank-shaft, which is more compact. It is evident from the diagram that the distance labeled "*x*" (the first nonbonded O−O distance) is reduced. Interestingly, the O−O radial distribution function in structure-I, -II, and -H clathrate hydrates resembles that of ice Ih, but in the tetragonal clathrate (TAC) it is strikingly similar to that of AMH II. This topology appears to be a stepping-stone on the route to more dense frameworks, such as ices II and III. The denser packing also results in a reduction of

(42) Speedy, R. J. *J. Phys. Chem.* **1984**, *88* (15), 3364–3373.
(43) Speedy, R. J.; Mezei, M. *J. Phys. Chem.* **1985**, *89* (1), 171–175.
(44) Ludwig, R.; Weinhold, F. *J. Chem. Phys.* **1999**, *110* (1), 508–515.
(45) Yokoyama, H.; Kannamia, M.; Kanno, H. *Chem. Phys. Lett.* **2008**, *463* (1−3), 99–102.
(46) Carrasco, J.; Michaelides, A.; Forster, M.; Haq, S.; Raval, R.; Hodgson, A. *Nat. Mater.* **2009**, *8*, 427–431.
(47) Hewat, A. W.; Riekel, C. *Acta Crystallogr.* **1979**, *A35*, 569–571.

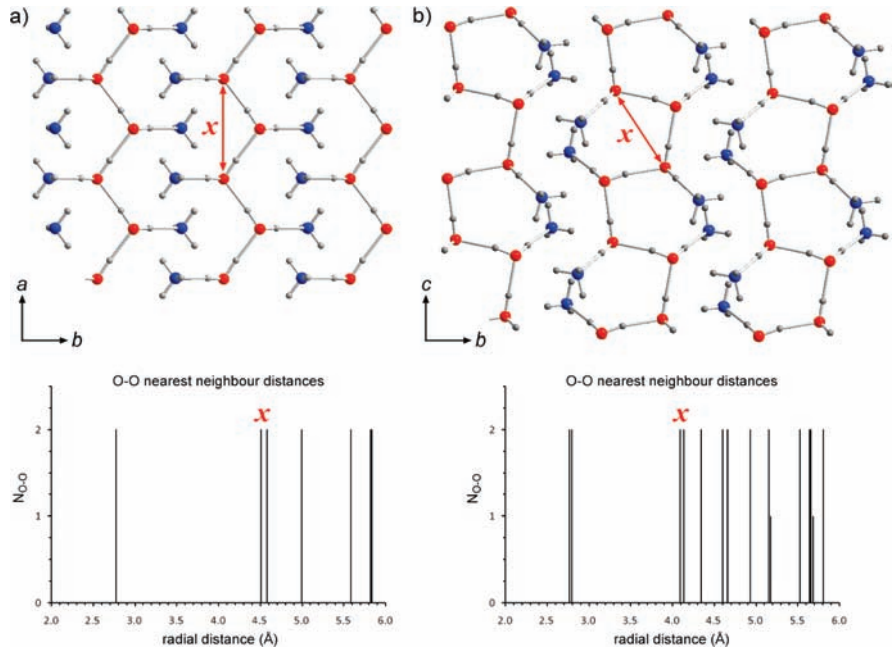

Figure 6. Comparison of the chain structures in AMH I (a) and AMH II (b) at the same spatial scale. Underneath each figure is a histogram of the O−O nearest neighbor distances for AMH I and II. The red arrow labeled with an "*x*" shows the length of the shortest nonbonded O−O contact and this is also marked on the histograms below.

nonbonded N−N distances (there are no *bonded* N−N contacts), the first shell shrinking from ∼3.95 Å down to as little as 3.31 Å.

Unexpectedly, the ammonia deuteron D1 appears not to be involved in a hydrogen bond. The nearest neighbors of D1 are an N1 atom at a distance of 2.58(2) Å, another N1 atom at a distance of 2.90(2) Å and an O2 atom also at a distance of 2.90(2) Å. The N-D···X angles formed by each of these putative contacts are, respectively, 146(1)°, 104(1)°, and 142(1)°. Given that the last two distances are significantly longer than the sum of the van der Waals radii of D and N (2.75 Å), or D and O (2.72 Å), and that all three of the proposed bonds are extremely bent, it is most unlikely that any of these contacts is a normal hydrogen bond. Indeed, it is noteworthy (though scarcely statistically significant) that the thermal displacement parameter of D1 is larger than that of any other deuteron, as one might expect of a nonbonded atom. The presence of a "dangling" deuteron is so far unique among the known ammonia hydrate structures, but is not uncommon; non-H-bonded hydrogen atoms occur, for example, in the structure of α-methanol[48] and methanol monoammoniate.[49]

Finally, there is the question of the hydrogen-bond ordering. While there is a clear preference for one particular ordering scheme in the experimental data, rather than the opposing scheme or a disordered model, it would still be desirable to obtain either 'better' powder data from a recovered specimen at limiting low temperatures (i.e., quenched to ambient pressure below ∼ 100 K, extracted and properly powdered, thereby eliminating any slight texture and/or coherent or incoherent background contributions from the pressure vessel), or *in situ* single crystal data. Until such time as that data is acquired, the phase diagram provides supporting evidence for a fully ordered structure. The Clapeyron slope of the AMH I → II phase boundary, dP/dT, appears to be zero. The 'tail' of measurements made by Hogenboom et al.[22] that is displaced to higher pressures at lower temperatures may be explained as the result of sluggish kinetics. Indeed, the same phenomenon is reported in the phase diagram of water ice by Gromnitskaya et al.[50] These authors show phase transitions on increase of pressure shifting to higher pressures as the temperature is reduced. Below 150−160 K, crystalline phase transitions may be inhibited altogether until compression is interrupted by the collapse of the structure to high-density amorphous ice. The inference of kinetic inhibition agrees with the observed persistence of AMH I to pressures of 3 GPa at temperatures of 115−150 K by Loveday and Nelmes.[24]

If the Clapeyron slope of the AMH I → II transition is zero, this implies that the entropy change is also zero. Since the greatest part of the entropy difference between ice phases is configurational entropy associated with hydrogen-bond disorder, then we may conclude that if AMH I is orientationally ordered and the AMH I → II Clapeyron slope is zero, then AMH II must also be orientationally ordered (*cf.*, ref 51).

4. Summary

We have used *ab initio* methods to make an experimentally constrained prediction of the high-pressure ammonia monohydrate II structure. Having subsequently collected high-quality neutron powder diffraction data from this phase, we have tested the *ab initio* model as well as applying a direct-space powder structure solution technique to the data. This work has demonstrated that the *ab initio* method was able to determine the structure correctly, with the exception that it produced one of two possible H-bond ordering schemes that is apparently not adopted by the real material. This is nonetheless a remarkable

(48) Torrie, B. H.; Weng, S.-X.; Powell, B. M. *Mol. Phys.* **1989**, *67* (3), 575–581.
(49) Fortes, A. D.; Wood, I. G.; Knight, K. S. *J. Appl. Cryst.* 2009. submitted.
(50) Gromnitskaya, E. L.; Stal'gorova, O. V.; Brazhkin, V. V.; Lyapin, A. G. *Phys. Rev. B* **2001**, *64*, article 094205.
(51) Fletcher, N. H. *Rep. Prog. Phys.* **1971**, *34* (3), 913–994.

success for the technique, as it represents the most complex molecular structure predicted to date using this method, and it is an example of the rapid progress being made in the field of molecular crystal structure prediction (e.g., ref 52).

Furthermore, with the exception of the very simple body-centered-cubic phases of ammonia monohydrate[53] and ammonia dihydrate,[14,54] this is the first published structure solution of any of the five AMH structures (II, III, IV, Va and Vb) and two ADH structures (II and IV) that are known to exist at present, and opens the door to understanding the molecular architecture of these phases as a function of pressure and temperature in the near future.

Acknowledgment. We gratefully acknowledge the Institut Laue-Langevin for beam time to conduct these experiments, and would like to thank the following ILL technical staff for their patience and hard work: Jean-Luc Laborier, Claude Payre, and Ludovic Gendrin. The authors thank Chris Goodway, team leader of the STFC ISIS Facility's Furnaces, Pressure, & Special Systems division, for assistance with gas handling and condensation of our ND_3 samples. ADF thanks I. G. Wood for discussions concerning the application of texture corrections in Rietveld refinement. ADF is funded by a STFC Advanced Fellowship, grant number PP/E006515/1.

Supporting Information Available: Supplementary Tables 1−3 and CIF data. This material is available free of charge via the Internet at http://pubs.acs.org.

JA9052569

(52) Day; Cooper, G. M.; Cruz-Cabeza, T. G.; Hejczyk, A. J.; Ammon, K. E.; Boerrigter, H. L.; Ammon,; Ammon, S. X. M.; Tan, J. S.; Della Valle, R. G.; Venuti, E. V.; Jose, J.; Gadre, S. R.; Desiraju, G. R.; Thakur, T. S.; van Eijck, B. P.; Facelli, J. C.; Bazterra, V. E.; Ferraro, M. B.; Hofmann, D. W. M.; Neumann, M. A.; Leusen, F. I. J.; Kendrick, J.; Price, S. L.; Misquitta, A. J.; Karamertzanis, P. G.; Welch, G. W. A.; Scheraga, H. A.; Arnautova, Y. A.; Schmidt, M. U.; van de Streek, J.; Wolf, A. K.; Schweizer, B. *Acta Crystallogr.* **2009**, *B65* (2), 107–125.

(53) Loveday, J. S.; Nelmes, R. J. *Phys. Rev. Lett.* **1999**, *83* (21), 4329–4332.

(54) Loveday, J. S.; Nelmes, R. J.; Bull, C. L.; Maynard-Casely, H. E.; Guthrie, M. *High Press. Res.* **2009**, *29* (3), 396–404.